A Map-Free Indoor Localization Method Using Ultrawideband Large-Scale Array Systems

Yilin Ji, Johannes Hejselbæk, Wei Fan, and Gert F. Pedersen

***Abstract*—In this letter, we propose a novel map-free indoor localization method using ultrawideband large-scale array systems in high-frequency bands. The proposed localization method comprises two stages, namely a channel-estimation stage and a target-localization stage. Due to the large array aperture, the locations of the scatterers associated to the multipath components can be estimated with the spherical wavefront model. The estimated scatterers are further used as virtual anchors to estimate the location of the target through trilateration. Since the scatterer locations are obtained from channel measurements, the map of the environment is not needed for localization. The proposed method is also assessed with measurements conducted in a cluttered indoor environment with line-of-sight (LoS) and non-LoS scenarios. Results show that the proposed algorithm attains good localization accuracy in both scenarios.**

***Index Terms*—Indoor localization, large-scale array systems, multipath-component estimation, ultrawideband.**

I. Introduction

INDOOR localization has always been attracting huge attention in both industry and academia due to its various applications. In the context of radio-based localization, many algorithms have been developed and can be categorized with respect to different criteria [1]. One such criterion is whether the underlying algorithm makes use of channel multipath components (MPCs). For algorithms only utilizing line-of-sight (LoS) components, the main drawback is that they do not work well in non-LoS (NLoS) scenarios, which limits their application in general-use cases. On the contrary, MPC-assisted algorithms exploit information from all MPCs for localization not only in LoS scenarios, but also in NLoS scenarios [2]–[4].

Another important criterion is whether it requires the map of the environment to perform localization. Since the map of an environment is not always easily available, and can be dynamic due to people walking or interior changes, a map-free algorithm becomes very helpful in this case. In the literature [2], [3], [5], a map-free algorithm called simultaneous localization and mapping (SLAM) was proposed. The SLAM algorithm is basically a recursive Bayesian filter that updates the state model and the observation model sequentially and recursively. However, a control vector consisting of motion information is needed to formulate the state model, so additional devices, e.g., accelerometers or gyroscopes, are required to provide relevant information.

In this letter, we propose a novel map-free indoor localization method using ultrawideband large-scale array systems at high-frequency bands. The proposed method comprises two stages, namely a channel-estimation stage and a target-localization stage. In the channel-estimation stage, parameters of the MPCs are estimated from measurements with the spherical wavefront model [6], [7]. In the target-localization stage, the locations of the scatterers in the environment are estimated with respect to the array location. The estimated scatterers are then used as virtual anchors to locate the target through trilateration.

The key differentiator of our method is that the virtual anchors are not derived from the image source method with respect to the map, but from the estimation of the physical scatterers in the environment instead. Therefore, the array location is the only geographical information needed to perform target localization. Moreover, the influence of people walking or interior changes is inherently conveyed in the changes of the virtual anchor locations, so the proposed method is also adaptive to dynamic environments. In addition, the proposed algorithm is assessed with measurements conducted in a cluttered room with both LoS and NLoS scenarios.

II. Proposed Localization Algorithm

A. Channel Representation and Parameter Estimation

A propagation channel can be assumed to be represented as the superposition of a number of MPCs. For a single-input–multiple-output (SIMO) system consisting of an M-element receive array, the time-invariant channel transfer function between the transmit antenna at the mth receive array element with $m \in [1, M]$ can be expressed as [8], [9]

$$H_m(f;\boldsymbol{\Theta}) = \sum_{l=1}^{L} H_m(f;\boldsymbol{\Theta}_l) \tag{1}$$

where f is the frequency, L is the number of MPCs, and $\boldsymbol{\Theta} = \{\boldsymbol{\Theta}_1, \ldots, \boldsymbol{\Theta}_L\}$ is the set of the parameters of all L MPCs. An illustration of the local coordinate system at the receive side is shown in Fig. 1. Considering the case where the aperture of the receive array is large enough that spherical wavefront is observed at the array, the contribution of the lth MPC at the mth

Manuscript received July 1, 2018; accepted July 30, 2018. Date of publication August 6, 2018; date of current version August 31, 2018. The work of W. Fan was supported in part by the Danish Council for Independent Research under Grant DFF611100525 and in part by the VIRTUSUO Project funded by the Innovation Fund Denmark. *(Corresponding author: Wei Fan.)*

The authors are with the Antenna Propagation and Millimeter-wave Systems Section, Department of Electronic Systems, Aalborg University, Aalborg 9100, Denmark (e-mail: yilin@es.aau.dk; joh@es.aau.dk; wfa@es.aau.dk; gfp@es.aau.dk).

Digital Object Identifier 10.1109/LAWP.2018.2863291

1536-1225 © 2018 IEEE. Personal use is permitted, but republication/redistribution requires IEEE permission.
See http://www.ieee.org/publications_standards/publications/rights/index.html for more information.

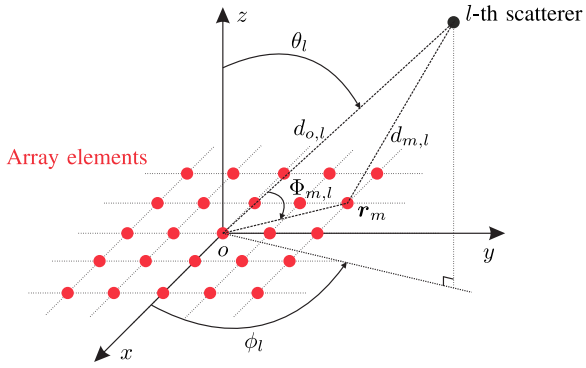

Fig. 1. Local coordinate system at the array side. Note that a uniform rectangular array is shown for illustration, and it can be replaced with arbitrary array structures in practice.

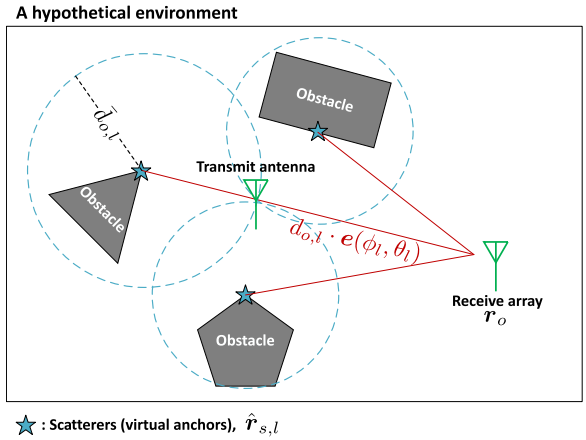

Fig. 2. Diagram of the proposed localization method. Physical obstacles are estimated as scatterers from measurements and are further used as virtual anchors to locate the transmitter.

receive array element can be written as

$$H_m(f;\boldsymbol{\Theta}_l) = \alpha_l \cdot \frac{g_m(f;\phi_l,\theta_l)}{4\pi f d_{m,l}/c} \cdot \exp\{-j2\pi f \tau_l\} \cdot \exp\{-j2\pi f(d_{m,l} - d_{o,l})/c\} \quad (2)$$

where $\boldsymbol{\Theta}_l = \{\alpha_l, \phi_l, \theta_l, d_{o,l}, \tau_l\}$ is the set of parameters of the lth MPC, including the complex amplitude, the azimuth angle of arrival, the elevation angle of arrival, the distance from the scatterer to the array center, and the delay, respectively. Furthermore, c is the speed of light, g_m is the antenna field pattern of the mth array element, and $d_{m,l}$ is the distance from the scatterer to the mth array element. The distance $d_{m,l}$ is calculated with the law of cosines as

$$d_{m,l} = \sqrt{d_{o,l}^2 + \|\boldsymbol{r}_m\|^2 - 2d_{o,l}\|\boldsymbol{r}_m\| \cos\Phi_{m,l}} \quad (3)$$

where $\|\cdot\|$ denotes the Euclidean norm operator, $\boldsymbol{r}_m$ is the coordinate vector of the mth array element, and $\Phi_{m,l}$ is the angle between the vector $\boldsymbol{r}_m$ and the direction of arrival with respect to the array center. $\cos\Phi_{m,l}$ can be explicitly expressed with $\boldsymbol{r}_m$ and a unit direction vector $\boldsymbol{e}(\phi_l,\theta_l) = [\cos\phi_l \sin\theta_l, \sin\phi_l \sin\theta_l, \cos\theta_l]$ as

$$\cos\Phi_{m,l} = \frac{\langle \boldsymbol{r}_m, \boldsymbol{e}(\phi_l,\theta_l)\rangle}{\|\boldsymbol{r}_m\|} \quad (4)$$

where $\langle\cdot,\cdot\rangle$ denotes the inner product operator. Note that $d_{o,l} = \tau_l \cdot c$ if the lth MPC corresponds to a LoS component.

By applying high-resolution channel estimation algorithms [7]–[9] to the channel measurements, it is possible to estimate the parameter set $\boldsymbol{\Theta}$ for all MPCs. Note that an array of a larger aperture size results in finer resolutions of the parameters $\{\phi_l, \theta_l, d_{o,l}\}$ for estimation and, hence, a smaller error in channel estimation and target localization.

B. Localization Principle

Two important assumptions are made for cluttered indoor high-frequency-band channels. We assume the following.

1) The estimated MPCs mainly consist of one-bounce links with or without LoS components depending on the scenarios.
2) Most of the estimated MPCs are induced by scattering from physical obstacles.

The first assumption can be made due to the high path loss at high-frequency bands and the limited dynamic range of measurement systems. The second assumption can be made due to the small wavelength at high-frequency bands, which becomes comparable to the size of physical obstacles in a typical cluttered indoor environment.

1) Physical Obstacles Identification: The transmit antenna and the physical obstacles are considered as the scattering sources in the environment. Essentially, the scatterers associated to the MPCs correspond to those scattering sources or, equivalently, to the transmit antenna and the physical obstacles in the environment. Once the parameters of MPCs are estimated, we can further estimate the locations of the scatterers in the environment. A diagram of the principle is shown in Fig. 2. With the knowledge of the receiver location, we can draw a line segment of length $d_{o,l}$ from the receive array center in the direction of $\boldsymbol{e}(\phi_l,\theta_l)$ for the lth MPC (shown as red lines). The lth scatterer is assumed to be located on the end of the line segment (shown as blue pentagrams). The location of the lth scatterer is then estimated as

$$\hat{\boldsymbol{r}}_{s,l} = \boldsymbol{r}_o + d_{o,l} \cdot \boldsymbol{e}(\phi_l,\theta_l) \quad (5)$$

where $\boldsymbol{r}_o$ is the coordinate vector of the receive array center.

Note that the true location of the lth scatterer in practice does not always coincide with the estimate calculated from (5). For example, if the surface of the physical obstacle is sufficiently large and flat compared to the wavelength, specular reflection occurs. In this case, the estimated scatterer location corresponds to the mirror image of its true location with respect to the reflection surface. On the other hand, objects such as metal frames or heating radiators, which can be usually found in indoor environments, induce scattering points on them. With the second assumption, the majority of the estimated scatterer locations coincide with their true locations in typical cluttered indoor environments, such as shopping malls, supermarkets, or warehouses.

2) Target Localization: The estimated scatterers are used as virtual anchors in the environment. With the first assumption, the majority of the estimated MPCs consist of one-bounce links

with or without an LoS component depending on the underlying scenario. The target location can be estimated through the optimization problem

$$\hat{\boldsymbol{r}}_t = \arg\min_{\boldsymbol{r}} \sum_{l=1}^{L} \left| \|\boldsymbol{r} - \hat{\boldsymbol{r}}_{s,l}\| - \bar{d}_{o,l} \right| \cdot P_l \tag{6}$$

where

$$\bar{d}_{o,l} = \tau_l \cdot c - d_{o,l} \tag{7}$$

is the residual propagation distance of the lth MPC between the lth scatterer and the transmit antenna (the radius of the dashed blue circumferences in Fig. 2), $\boldsymbol{r}$ is the coordinate vector of an arbitrary point in the space, $P_l = \|\alpha_l \cdot \frac{c}{4\pi f d_{o,l}}\|^2$ is the power of the lth MPC, and $|\cdot|$ denotes the absolute value operator. Equation (6) can be solved efficiently through coarse-to-fine search techniques.

A high localization accuracy is expected when the scatterers are well separated in space around the target, as shown in Fig. 2. However, when the scatterers are located closely, the accuracy of trilateration deteriorates. It is also worth mentioning that the validity of the localization principle is based on the validity of the two important assumptions made for high-frequency-band channels in cluttered indoor environments. Therefore, the performance of the proposed localization method is expected to deteriorate in the cases where the two assumptions do not hold well, e.g., at low-frequency bands or in empty rooms where specular reflections are dominant.

III. Experimental Evaluation

A. Measurement Campaign

The measurements were conducted in an indoor environment with a vector network analyzer (VNA)-based channel sounder [6]. The SIMO channels were measured with a horn antenna on the transmit side and a virtual uniform circular array (UCA) on the receive side. The virtual UCA was formed by mounting a biconical antenna on a turntable with a radius of 25 cm stepping every 1° in the azimuth plane. The horn antenna has a half-power beamwidth of 54° in the azimuth plane, and an antenna gain of 10 dBi. Both the transmit antenna and the receive antenna were placed 1 m above the floor. The channel frequency responses were measured with 1500 frequency points evenly over 26–30 GHz, which corresponds to a range (i.e., delay times speed of light) resolution of 7.5 cm. The floor plan of the environment is shown in Fig. 3. In total, 42 receiver positions were measured along a reference line (red) with 20 cm spacing. The centers of the receive arrays for these positions are depicted as green dots. Single-channel snapshots were measured at most of those positions, and multiple-channel snapshots were measured in the 1 cm vicinity of positions 1, 23, 32, and 41, which are denoted as green dots surrounded by blue rings, as shown in Fig. 3. With respect to the transmit antenna position, the receiver moves from the LoS region to the NLoS region as the position index increases. Detailed descriptions of the measurement campaign can be found in [6].

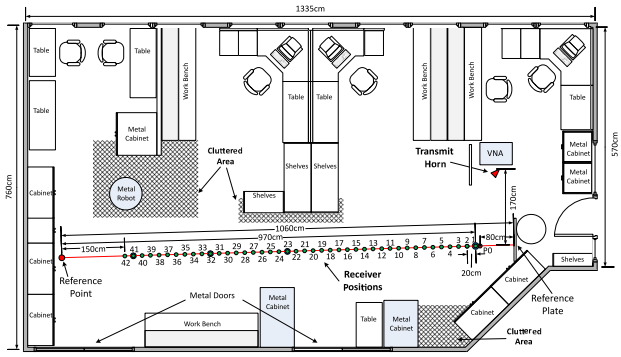

Fig. 3. Floor plan of the measurement environment and the 42 receiver positions. The centers of the receive arrays are depicted as green dots.

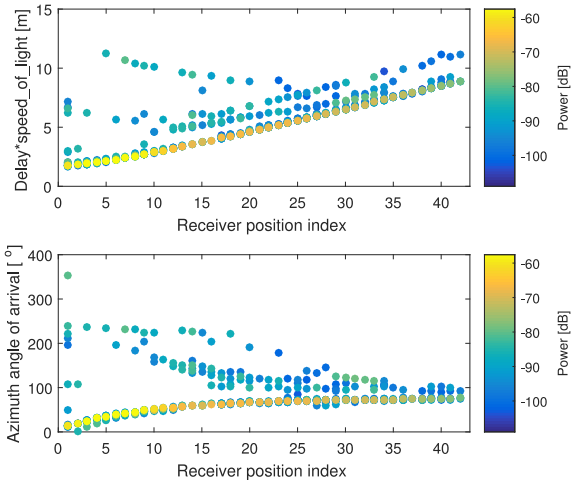

Fig. 4. Estimated MPCs against receiver positions in the propagation distance and the azimuth angle of arrival domain.

B. Results Analysis

The channel measurement data are processed with a maximum likelihood estimator [7] to extract the MPCs, and the estimation results for all receiver positions are presented in Fig. 4. It shows that as the receiver position index increases, the power of the LoS component becomes weaker, which indicates the underlying channel is turning from the LoS to the NLoS. In addition, the azimuth angles of arrival of the MPCs converge to a confined region around 90°. Since the proposed localization algorithm utilizes the spatial richness of the channel, it may probably lead to a deterioration in the localization accuracy.

The localization results at receiver positions 23 and 39 are shown in Fig. 5 as the examples for the LoS and the NLoS scenarios, respectively. For position 23 [see Fig. 5(a)], we can see the scatterer corresponding to the LoS component is estimated at the transmitter location. In addition, the circumferences of the other MPCs also intersect around the true transmitter location, which leads to high estimation accuracy. For position 39 [see Fig. 5(b)], the circumferences of most MPCs still intersect around the true transmitter location. However, due to the decreased spatial richness at position 39 as shown in Fig. 4, the localization is less accurate than that at position 23.

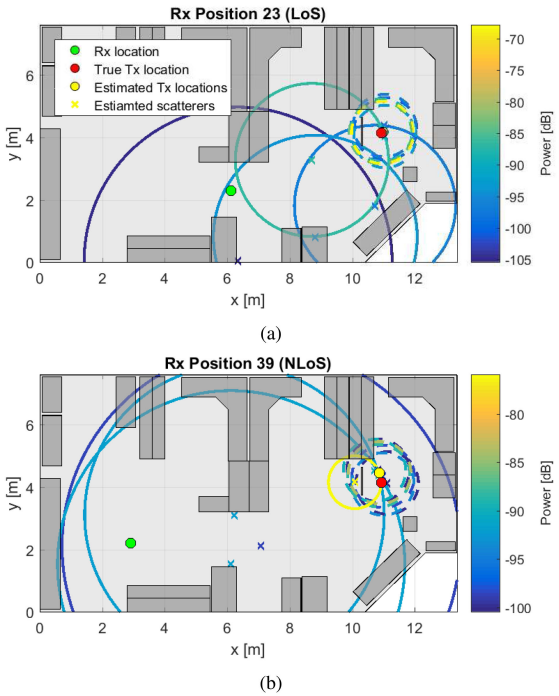

Fig. 5. Localization results at receiver (Rx) positions 23 and 39. The range of the transmitter (Tx) with respect to the lth scatterer is shown as a solid circumference with its radius equal to $\bar{d}_{o,l}$. Note when $\bar{d}_{o,l} = 0$, dashed circumferences with 1 m radius are shown for visualization. The color of the circumferences and crosses represents the power of the MPCs.

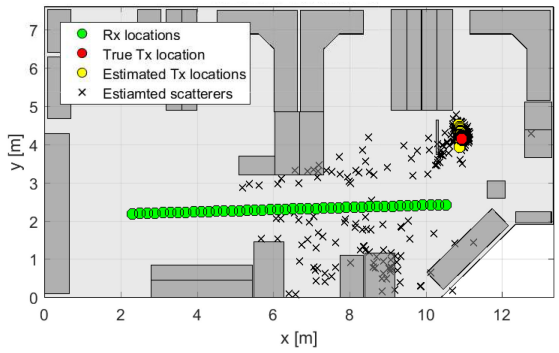

Fig. 6. Estimated transmitter locations $\hat{\boldsymbol{r}}_t$ and the estimated scatterer locations $\hat{\boldsymbol{r}}_{s,l}$ for all 42 receiver positions superimposed.

The results for all 42 positions are shown in Fig. 6. We can see the majority of the estimated transmitter locations are close to the true location. The estimated scatterer locations for all receiver positions are also superimposed in Fig. 6. We can see that some of the estimated scatterers are surrounding the true transmitter location. This is because the scatterers associated to the LoS components correspond to the transmitter itself. The rest of the estimated scatterer locations are either close to the physical obstacles or corresponding to the ground reflection along the propagation paths.

Furthermore, the error distance between the true location of the transmit antenna $\boldsymbol{r}_t$ and the estimated location $\hat{\boldsymbol{r}}_t$ is calculated as $\varepsilon = \|\boldsymbol{r}_t - \hat{\boldsymbol{r}}_t\|$. The resulting error distances for the 42 receiver positions are shown in Fig. 7. It shows a trend that the error distance increases with the position index, which is in agreement with the discussion for Fig. 4. Nevertheless, the

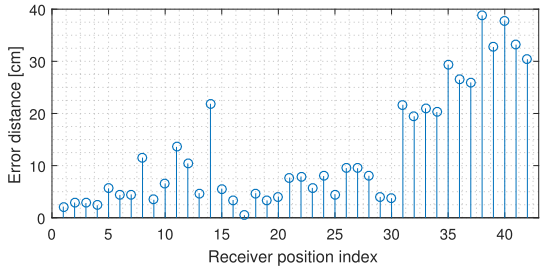

Fig. 7. Error distance ε obtained over the 42 receiver positions. The results shown here are obtained with single-channel snapshots.

TABLE I
ERROR DISTANCES (UNIT: cm) IN THE VICINITY OF POSITIONS WITH MULTIPLE CHANNEL SNAPSHOTS

Position Index	#1	#23	#32	#41
Snapshot 1	2.15	5.73	20.56	33.20
Snapshot 2	6.31	4.42	19.46	70.94
Snapshot 3	2.39	4.42	–	72.89
Composite	3.11	4.57	19.99	12.41

location of the transmit antenna is still well estimated, and the majority of the error distances are below 30 cm, which is around four times the underlying range resolution.

Note that the error distances shown in Fig. 7 are obtained from single-channel snapshots. One potential reason for the large error distances at these singular positions can be due to the lack of channel snapshots. Therefore, the error distance is further calculated at the positions where multiple channel snapshots were measured in their 1 cm vicinity. The corresponding error distances at those positions are given in Table I. It shows a slight move of the receiver position may introduce larger variation in localization results for the NLoS scenario than for the LoS scenario. The composite error distance is further calculated with respect to the mean location of $\hat{\boldsymbol{r}}_t$ over multiple snapshots. It also shows averaging results from multiple snapshots helps us to improve the localization accuracy for the NLoS scenario, e.g., at position 41.

IV. CONCLUSION

In this letter, we propose a map-free indoor localization method utilizing ultrawideband large-scale array systems in high-frequency bands. Given that massive multiple-input–multiple-output systems and high-frequency bands are assumed to be deployed in the fifth-generation communication systems, the proposed indoor localization method can be implemented directly with the setups of the upcoming communication systems. In the proposed method, scatterers in the environment are utilized as virtual anchors to estimate target locations. The advantage of this method is that it does not rely on the map of the environment to perform target localization. The performance of the proposed method is also assessed with measurements conducted in a cluttered room including both LoS and NLoS scenarios. The results show that the error of the estimated target location increases with the distance between the transmitter and the receiver, but the majority of the estimation error is below 30 cm.

REFERENCES

[1] P. Meissner, "Multipath-assisted indoor positioning," Ph.D. dissertation, Dept. Signal Process. Speech Commun. Laboratory, Graz Univ. Technol., Graz, Austria, 2014.

[2] K. Witrisal *et al.*, "High-accuracy localization for assisted living: 5G systems will turn multipath channels from foe to friend," *IEEE Signal Process. Mag.*, vol. 33, no. 2, pp. 59–70, Mar. 2016.

[3] C. Gentner, T. Jost, W. Wang, S. Zhang, A. Dammann, and U. C. Fiebig, "Multipath assisted positioning with simultaneous localization and mapping," *IEEE Trans. Wireless Commun.*, vol. 15, no. 9, pp. 6104–6117, Sep. 2016.

[4] B. Hanssens *et al.*, "An indoor variance-based localization technique utilizing the UWB estimation of geometrical propagation parameters," *IEEE Trans. Antennas Propag.*, vol. 66, no. 5, pp. 2522–2533, May 2018.

[5] T. Bailey and H. Durrant-Whyte, "Simultaneous localization and mapping (SLAM): Part I," *IEEE Robot. Automat. Mag.*, vol. 13, no. 2, pp. 99–110, Jun. 2006.

[6] J. Hejselbæk, Y. Ji, W. Fan, and G. F. Pedersen, "Channel sounding system for mm-Wave bands and characterization of indoor propagation at 28 GHz," *Int. J. Wireless Inf. Netw.*, vol. 24, no. 3, pp. 204–216, 2017.

[7] Y. Ji, W. Fan, and G. F. Pedersen, "Channel estimation using spherical-wave model for indoor LoS and obstructed LoS scenarios," in *Proc. 11th Eur. Conf. Antennas Propag.*, 2017, pp. 2459–2462.

[8] Y. Wang, J. Li, P. Stoica, M. Sheplak, and T. Nishida, "Wideband RELAX and wideband CLEAN for aeroacoustic imaging," *J. Acoust. Soc. Amer.*, vol. 115, no. 2, pp. 757–767, 2004.

[9] K. Haneda, J. I. Takada, and T. Kobayashi, "A parametric UWB propagation channel estimation and its performance validation in an anechoic chamber," *IEEE Trans. Microw. Theory Techn.*, vol. 54, no. 4, pp. 1802–1811, Jun. 2006.